Tunability of non-plasmon resonances in e-polarized terahertz wave scattering from microsize graphene strip-on-substrate gratings

Fedir O. Yevtushenko, Sergii V. Dukhopelnykov, Yuriy G. Rapoport, Tatiana L. Zinenko, Ronan Sauleau, Alexander I. Nosich

Research Article | Vol. 13, No. 8 / 1 Aug 2023 / Optical Materials Express 2274
Optical Materials EXPRESS

Tunability of non-plasmon resonances in e-polarized terahertz wave scattering from microsize graphene strip-on-substrate gratings

FEDIR O. YEVTUSHENKO,[1,*] SERGII V. DUKHOPELNYKOV,[1,2,3] YURIY G. RAPOPORT,[4] TATIANA L. ZINENKO,[1] RONAN SAULEAU,[3] AND ALEXANDER I. NOSICH[1]

[1]*Laboratory of Micro and Nano Optics, Institute of Radio-Physics and Electronics NASU, Kharkiv, 61085, Ukraine*
[2]*Department of Applied Mathematics, V. N. Karazin Kharkiv National University, Kharkiv, 61022, Ukraine*
[3]*Institute of Electronics and Numerical Technologies, Universite de Rennes, Rennes 35042, France*
[4]*Space Radio-Diagnostic Research Centre, University of Warmia and Mazury, 10-720 Olsztyn, Poland*
[*]*fedir.yevtushenko@gmail.com*

Abstract: We consider the scattering and absorption of the E-polarized plane wave by the infinite grating of flat graphene strips lying on flat dielectric substrate. To build a trusted full-wave meshless algorithm, we cast the scattering problem to the dual series equations and perform its analytical regularization based on the use Inverse of Discrete Fourier Transform. Then, the problem reduces to a Fredholm 2nd-kind matrix equation for the unknown Floquet harmonic amplitudes. Therefore, the convergence of the resulting code is guaranteed by the Fredholm theorems. Numerical experiments show that such a configuration is a frequency-selective metasurface or one-periodic photonic crystal. If the grating period and substrate thickness are micrometer-sized, the resonance frequencies of such a cavity are in the terahertz range. As plasmon modes are absent in the E-polarization case, these resonances correspond to low-Q slab modes of the substrate, slightly perturbed by the presence of grating, and ultrahigh-Q lattice modes of the whole grating as a periodic open cavity. We quantify their effect both using our full-wave numerical code and deriving the asymptotic analytical expressions for the lattice-mode frequencies and Q-factors.

1. Introduction

Today, the focus of research into graphene as new material has shifted to the design of electrically tunable electromagnetic-wave devices and systems, in wide range from terahertz to infrared frequencies [1–4]. This means that instead of infinite sheets of graphene, various configurations of patterned graphene, strips, disks and more complicated shapes, are measured and modeled. Needless to explain that all fabricated and measured graphene samples have finite dimensions. As known, graphene has high conductivity tunable with the aid of DC bias, and its surface impedance is inductive that enables the existence of surface plasmon natural modes on the finite-size graphene samples, in the terahertz and infrared ranges [5]. Therefore, their resonance frequencies are also tunable, in wide range.

However, surface plasmon modes on graphene samples have their fields with magnetic component predominantly in the graphene plane and the electric field component – predominantly normal to that plane. In the two-dimensional (2-D) case this means that patterned-graphene plasmon modes are always H-polarized (magnetic field being parallel to the strips), and no such E-polarized (electric field being parallel to the strips) modes exist. In particular, this is true for the most practically important configuration – graphene strip grating, which is already exploited as the key component of mid-infrared bio and chemo-sensors [3,4,6–11]. As a result, the bulk

#496037 https://doi.org/10.1364/OME.496037
Journal © 2023 Received 24 May 2023; revised 29 Jun 2023; accepted 29 Jun 2023; published 18 Jul 2023

Optical Materials EXPRESS

of the publications on graphene strip gratings as frequency-selective scatterers deal with the H-polarization [8–13]. The E-polarization scattering was briefly considered in [8,9] and in greater details, however, within quasi-static approximation and using the circuit theory, in [14].

Hence, it is necessary to improve the understanding of the scattering and absorption characteristics of graphene-strip gratings in the E-polarization regime. This explains the subject and goals of our work: we study the scattering and absorption of the E-polarized plane wave by on-substrate grating of graphene strips in the full-wave formulation and using a convergent numerical code.

As the plasmon modes and associated resonances are absent in this case, one of the interesting questions is how the tunability of graphene can influence the frequencies and sharpness of non-plasmon mode resonances. In the analysis we use the Method of Analytical Regularization (MAR) [15] based on the Inverse Discrete Fourier Transform (IDFT). This technique was originally developed for the analysis of gratings made of resistive strips in the free space [16]. A different version was applied to the scattering from the graphene-strip grating symmetrically embedded into a dielectric slab [9]. Its huge advantage before less sophisticated numerical treatments and commercial codes is the mathematically guaranteed convergence, which follows from the Fredholm theorems.

However, the most practical configuration is a strip grating not embedded into a dielectric layer but lying on the surface of such layer. Therefore, in our work we had to modify MAR-IDFT to account for the flat dielectric layer located below the grating. The MAR-IDFT technique is remarkable for the absence of numerical integrations needed to fill in the resulting matrix equation. This is in contrast to the other MAR-like techniques, which use singular integral equations solved by the Galerkin method with the polynomial basis [17–19].

The lattice modes, which are in the focus of our study, need a short introduction. They exist in nearly all periodic open resonators, however, have received no attention or been overlooked until the 2000s; sometimes, they have been misinterpreted because of their ultra-large Q-factors and extreme closeness to the Rayleigh Anomalies (RAs). Most probably, they were first time revealed in [20] on the periodically modulated impedance plane, however, they were largely forgotten later. Now, they are intensively studied and find important applications [3,9–13,21–25]. As known, if the periodicity is vanishing, their complex-valued natural frequencies approach the purely real-valued values and hence their Q-factors tend to infinity. As a consequence, accurate quantification of the ultra-fine lattice-mode resonances is a huge challenge for the existing commercial codes. In contrast, our MAR-based full-wave meshless algorithm is fully adequate to that task [9,13]. Besides the lattice modes, the considered metasurface supports the slab modes of the dielectric substrate that are slightly perturbed by the presence of strips and have low Q-factors.

In computations, the results of which are presented below, we consider the micrometer-size strip width, substrate thickness and grating period. Then the frequencies of both the slab modes and the lattice modes lie in the terahertz range.

2. Formulation, dual series equations and Fredholm matrix equations

Figure 1 shows the cross-section of infinite flat grating of zero-thickness graphene strips with period p, located in the plane $y = 0$. This plane is the upper surface of a homogeneous dielectric layer (substrate) of relative dielectric permittivity ε and thickness h. The graphene strips are assumed infinite along the z-axis and have the width d.

In the case of the E-polarization, the field components are $(0, 0, E_z)$ and $(H_x, H_y, 0)$. It is convenient to choose E_z as the "basic" component; we denote it $U(x, y)$. The time-harmonic ($e^{-i\omega t}$) E-polarized plane wave is incident on the grating-covered side of substrate at the angle α counted from the x-axis.

$$U^{in}(x, y) = e^{-ik_0 y \sin\alpha - ik_0 x \cos\alpha}, \quad y>0, \tag{1}$$

Optical Materials EXPRESS

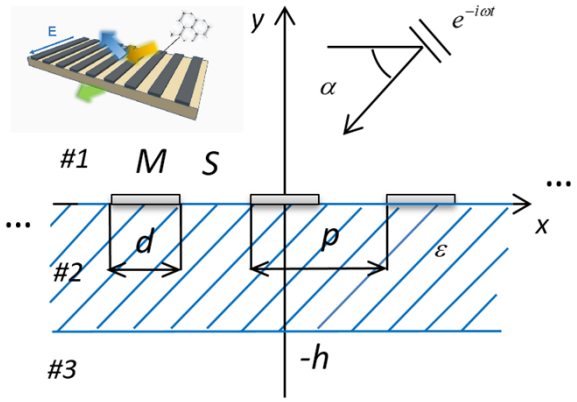

Fig. 1. Cross-section of infinite graphene strip grating on dielectric substrate, excited by an E-polarized plane wave.

where $k_0 = \omega/c = \omega(\varepsilon_0\mu_0)^{1/2}$. We decompose the total field as a sum, $U^{tot} = U^{in} + U^{(1)}$, in the domain #1, and $U^{tot} = U^{(2,3)}$ in the domains ##2,3. Thus, we obtain the following boundary value problem for determining the function $U = U^{(j)}$, $j = 1, 2, 3$: it must satisfy (I) the 2-D Helmholtz equation everywhere outside the strips and the slab interfaces,

$$[\nabla^2 + k_0^2\varepsilon^{(j)}]U^{(j)}(\vec{r}) = 0, \quad j = 1, 2, 3, \tag{2}$$

where we imply $\varepsilon^{(1)} = \varepsilon^{(3)} = 1$, $\varepsilon^{(2)} = \varepsilon$, (II) the set of the boundary conditions, which contain the total E-field continuity condition across the whole interfaces at $y = 0$ and $y = -h$, the dual conditions for the tangential total H field at the strip (M) and slot (S) intervals of $y = 0$: resistive-type boundary condition (see [5]) at the strips, $\vec{r} \in M : \{y = 0;\ |x + np| < d/2;\ n = 0, \pm1, \pm2, \ldots\}$,

$$[U^{(2)}(x, 0) + U^{(in)}(x, 0) + U^{(1)}(x, 0)] = -2Z\frac{1}{ik_0}\frac{\partial}{\partial y}[U^{(2)}(x, y) - U^{(in)}(x, y) - U^{(1)}(x, y)]\Big|_{y=0}, \tag{3}$$

where Z is the surface impedance of graphene, normalized by the free-space impedance, Z_0 (see Section 3), and the continuity condition at the slots, $\vec{r} \in S : \{y = 0; -\infty < x < +\infty\}\backslash M$,

$$\partial[U^{(2)}(x, y) - U^{(in)}(x, y) - U^{(1)}(x, y)]/\partial y|_{y=0} = 0, \tag{4}$$

and similar to (4) condition at the whole lower interface, $y = -h$, $-\infty < x < +\infty$, (III) the radiation condition at $y \to \pm\infty$ that demands the functions $U^{(1)}$ and $U^{(3)}$ to contain only the waves propagating away from the grating, and (IV) the condition of local finiteness of power [15]. Conditions (I)–(IV) guarantee that the solution is unique.

The property of quasi-periodicity, $U^{(j)}(x + p, y) = e^{ikx\cos\alpha}U^{(j)}(x, y)$ $(j = 1, 2, 3)$ is enforced by the incident plane wave and the periodicity of the boundary conditions. It allows expanding the unknown field in terms of the Floquet series in each domain. On introducing the dimensionless notations, $\phi = 2\pi x/p$, $\psi = 2\pi y/p$, $\theta = \pi d/p$, $\xi = 2\pi h/p$, $\kappa = p/\lambda$, $s = d/p$, we write these expansions as follows:

$$U^{(1)} = \sum_{n=-\infty}^{+\infty} a_n e^{i(\gamma_n\psi + \beta_n\phi)}, \quad \psi > 0, \tag{5}$$

$$U^{(2)} = \sum_{n=-\infty}^{+\infty} (b_n e^{i\gamma_n^{sl}\psi} + c_n e^{-i\gamma_n^{sl}\psi})e^{i\beta_n\phi}, \quad 0 > \psi > -\xi, \tag{6}$$

Optical Materials EXPRESS

$$U^{(3)} = \sum_{n=-\infty}^{+\infty} d_n e^{i(-\gamma_n \psi + \beta_n \phi)}, \quad \psi < -\xi, \tag{7}$$

where unknown coefficients a_n, b_n, c_n, d_n are the amplitudes of Floquet harmonics, and other notations are $\gamma_0 = \kappa \sin\alpha$, $\beta_0 = \kappa \cos\alpha$, $\beta_n = n - \beta_0$, $\gamma_n = (\kappa^2 - \beta_n^2)^{1/2}$, $\gamma_n^{sl} = (\kappa^2 \varepsilon - \beta_n^2)^{1/2}$. Then the reflectance and transmittance, in terms of power, are expressed as

$$P_{ref} = \gamma_0^{-1} \sum_{|n-\kappa\cos\beta|<\kappa} \gamma_n |a_n|^2, \quad P_{tr} = \gamma_0^{-1} \sum_{|n-\kappa\cos\beta|<\kappa} \gamma_n |d_n|^2. \tag{8}$$

The power absorbed in the metasurface can be found directly, by integrating the squared strip current (see [9,10]), or by using the power conservation law, $P_{abs} = 1 - P_{ref} - P_{tr}$.

Note that (5)–(7) already satisfy the conditions (I) and (III). The boundary conditions, valid on the whole upper and lower interfaces, allow excluding a part of unknown coefficients. Then, the dual conditions (3) and (4) generate a dual series equation (DSE), with the domains of validity M and S. On introducing new unknowns, $A_n = \delta_{0n}(1 - 2\kappa \sin\alpha/\Gamma_0) + a_n$, and denoting

$$\Gamma_n = \gamma_n - \gamma_n^{sl} \frac{(\gamma_n^{sl} - \gamma_n) e^{i\gamma_n^{sl}\xi} - (\gamma_n^{sl} + \gamma_n) e^{-i\gamma_n^{sl}\xi}}{(\gamma_n^{sl} - \gamma_n) e^{i\gamma_n^{sl}\xi} + (\gamma_n^{sl} + \gamma_n) e^{-i\gamma_n^{sl}\xi}}, \tag{9}$$

we follow [16] and cast the DSE to the following form:

$$\sum_{n=-\infty}^{\infty} A_n \Gamma_n e^{i\beta_n \phi} = \begin{cases} 0, & \theta < |\phi| < \pi \\ -\frac{\kappa}{Z} \sum\limits_{n=-\infty}^{\infty} A_n e^{i\beta_n \phi} - \frac{2\kappa^2 \sin\alpha}{Z\Gamma_0} e^{i\beta_0 \phi}, & |\phi| < \theta \end{cases} \tag{10}$$

The left hand part of (10) can be inverted analytically using the IDFT and the orthogonality of the exponents, thus yielding a matrix equation for the unknowns A_n. However, the rate of decay of the obtained by IDFT matrix elements with larger $|m|$ and $|n|$ is different, namely $O(m^{-2})$ and $O(|n|^{-1})$. To balance it, we follow [16] and introduce new variables as

$$x_n = A_n w_n, \quad w_n = \sqrt{|n| + 1}, \tag{11}$$

and finally arrive at the infinite matrix equation as follows:

$$x_m + \frac{\kappa w_m}{Z\Gamma_m} \sum_{n=-\infty}^{\infty} \frac{S_{mn}}{w_n} x_n = -\sin\alpha \frac{2\kappa^2}{Z\Gamma_0} \frac{S_{m0} w_m}{\Gamma_m}, \tag{12}$$

where

$$S_{nm} = \frac{\sin(n-m)\theta}{\pi(n-m)}, \quad S_{mm} = \frac{\theta}{\pi}, \quad m, n = 0, \pm 1, \pm 2, \ldots \tag{13}$$

As $\Gamma_n \cong i|n|[1 + O(e^{-|n|2\pi h/p}) + O(\kappa^2/|n|)]$ if $n >> 1$, inspection of the large-index behavior of the matrix elements enables us to state that Eq. (12) is a Fredholm second kind matrix equation in the space of number sequences l_2. Hence, the convergence of its numerical solution to the exact solution with larger truncation numbers N is mathematically guaranteed by the Fredholm theorems. Then, the accuracy is easily controlled with the aid of the matrix truncation order.

3. Graphene's surface conductivity and impedance

The most widely adopted today quantum model of the electron mobility in graphene monolayer is the Kubo model [5]. Here, the graphene thickness is considered zero, and its surface conductivity

Optical Materials EXPRESS

$\sigma(\omega, \mu_c, \tau, T)$ depends on the cyclic frequency ω, chemical potential μ_c, electron relaxation time τ and temperature T. The conductivity consists of the intraband term,

$$\sigma_{\text{intra}} = \frac{q_e^2 k_B T}{\pi\hbar^2(1/\tau - i\omega)} \left\{ \frac{\mu_c}{k_B T} + 2\ln\left[1 + \exp\left(-\frac{\mu_c}{k_B T}\right)\right]\right\}, \tag{14}$$

and the interband one, which has a simple approximation, valid at $\mu_c >> k_B T$ [5],

$$\sigma_{\text{inter}} = \frac{iq_e^2}{4\pi\hbar} \ln\frac{2|\mu_c| - (\omega + i\tau^{-1})\hbar}{2|\mu_c| + (\omega + i\tau^{-1})\hbar} \tag{15}$$

where q_e is the charge of the electron, k_B is the Boltzmann constant, and $\hbar$ is the reduced Planck constant. Due to the fact that ImZ<0, graphene can support the propagation of the plasmon wave [5]. Then, the normalized surface impedance of graphene is

$$Z(\omega) = Z_0^{-1}(\sigma_{\text{intra}} + \sigma_{\text{inter}})^{-1} \tag{16}$$

Inspection of (14) and (15) shows (see [26]) shows that the interband conductivity, in absolute value, is much smaller than the intraband one, which is also called the Drude model, in the wide range from the statics to the far infrared light where the upper frequency bound, f_c, scales with the chemical potential. For instance, if $\tau = 1$ ps, $T = 300$ K, and $\mu_c = 0.25$ eV, then $|\sigma_{\text{inter}}| \le 0.1|\sigma_{\text{intra}}|$ at the frequencies up to 40 THz, while if $\mu_c = 0.39$ eV, then the same is valid at the frequencies up to 60 THz. Provided that σ_{inter} can be neglected, the normalized surface impedance (or resistivity) of graphene can be taken as follows:

$$Z(\omega) \approx (Z_0\sigma_{\text{intra}})^{-1} = (1/\tau - i\omega)\Omega^{-1}, \tag{17}$$

$$\Omega = \frac{q_e^2 k_B T Z_0}{\pi\hbar^2} \left\{ \frac{\mu_c}{k_B T} + 2\ln\left[1 + \exp\left(-\frac{\mu_c}{k_B T}\right)\right]\right\}, \tag{18}$$

where Ω does not depend on the frequency. Still, at the near infrared and visible light frequencies, the description of the surface conductivity of graphene should take into account both types of conductivity.

Below, we will use full expression (16) in the numerical analysis and simplified expression (17) in the analytical description of the lattice mode resonance frequencies.

4. Numerical results: slab mode and lattice mode resonances

For numerical experiments, we choose the graphene parameters as follows: $\mu_c = 0.39$ eV, $T = 300$ K, and electron relaxation time $\tau = 1$ ps. The latter value is rather optimistic, however, it helps to emphasize the lattice-mode resonances. Note that today the largest values of graphene's chemical potential, achieved with the best available samples, are around 1 eV.

In Fig. 2, we show the frequency dependences of the reflectance (a) and absorbance (b) of the studied metasurface in the range from zero to 10 THz, in the case of the normal incidence.

In computations, we use the matrix Eq. (12) truncated to $N = 50$. The transmittance can be found from the power conservation law, $T = 1 - R - A$, and is not shown. Here, the grating has period of $p = 70$ μm, the strip width is $d = 14$ μm, and the substrate thickness is $h = 10$ μm. Thus, both the filling factor of the grating and the relative thickness of the substrate are rather small, $d/p = 0.2$ and $h/p = 0.143$, respectively. The substrate relative dielectric permittivity is 1 (i.e. the grating is suspended in free space), 2.25 and 4.2.

On the plots, one can see several sharp Fano-shape double-extremum peaks, overlapping with a sinus-like background. These are the ultrahigh-Q lattice-mode $L_{10}{}^{+}$ and $L_{20}{}^{+}$ resonances on the background of low-Q slab-mode resonances S_0, S_1, and S_2. The positions of the lattice-mode

Optical Materials EXPRESS

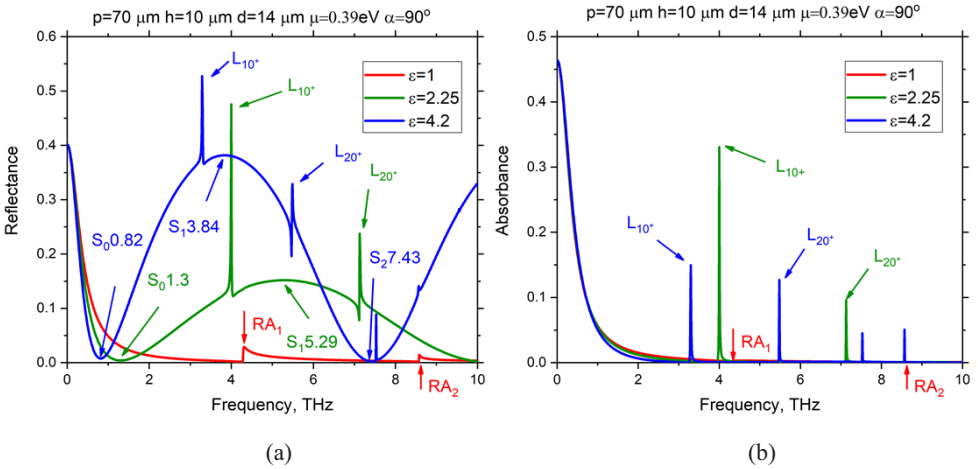

Fig. 2. The reflectance (a) and absorbance (b) of the suspended and on-substrate gratings with period $p = 70$ μm, filling factor $d/p = 0.2$, and relative substrate thickness $h/p = 1/7$, versus the frequency for three values of substrate permittivity, $\varepsilon = 1$,2.25 and 4.2.

peaks are defined by the period and mediated by the wavelength of the principal guided wave TE_0 of the dielectric-slab substrate - see [9,10,22] and Section 5 below. They are always shifted to the red side of the RAs, the first two pairs of which (for the normal incidence, ± 1-st and ±2-nd) correspond to $\kappa = 1$ and 2 and lie at 4.286 THz and 8.572 THz, respectively. The shift from RA gets larger for larger optical contrast and thickness of the substrate and larger mode index, m, which corresponds to the RA index. Note that, for the graphene strip grating suspended in the free space, no resonance peaks of reflectance are observed, however, there are sharp drops of both transmittance and absorbance at the RA frequencies.

Wide bell-like peaks of reflectance in Fig. 2-(a) are located at 3.84 THz for $\varepsilon = 4.2$ and at 5.29 THz for $\varepsilon = 2.25$. As mentioned, they correspond to the lowest y-odd mode, S_1, of the slab as a Fabry-Perot resonator, slightly perturbed by the presence of strips. They are absent on the plots of absorbance in Fig. 2-(b) as the slab is assumed lossless. The broad minima of reflectance are also associated with the slab modes, however, those which have the y-even E-fields when the strips are absent. The lowest of them is S_0, which has zero frequency in the absence of strips; the appearance of strips makes its frequency finite.

In Fig. 3, we show in-resonance total electric field portraits computed at the frequencies of the absorbance peaks corresponding to the x-even lattice modes $L_{10}{}^+$ and $L_{20}{}^+$. Here, the graphene strips are marked as white straight lines and the dielectric-air boundaries are shown as white dotted lines.

The panels (a) and (b) are for the substrate with permittivity 2.25 and the panels (c) and (d) – with permittivity 4.2. They demonstrate the standing-wave patterns both above the grating and in the normal direction. In the $+y$ direction, the standing wave appears due to strong reflection of the incident plane wave. The standing wave along the grating is the signature of the corresponding natural lattice mode: two (for $L_{10}{}^+$) and four (for $L_{20}{}^+$) bright spots on the period. This is because in the lattice-mode resonances, at the normal incidence, the near field is heavily dominated by the contribution of two Floquet harmonics, namely, ± 1-st and ±2-nd, respectively, see Eq. (4) in [22]. Note that these harmonics remain non-propagating away from the grating, and their in-resonance amplitudes scale with lattice-mode Q-factors. This means that they can be arbitrarily large if the periodicity vanishes because then the frequencies tend to purely real values.

Optical Materials EXPRESS

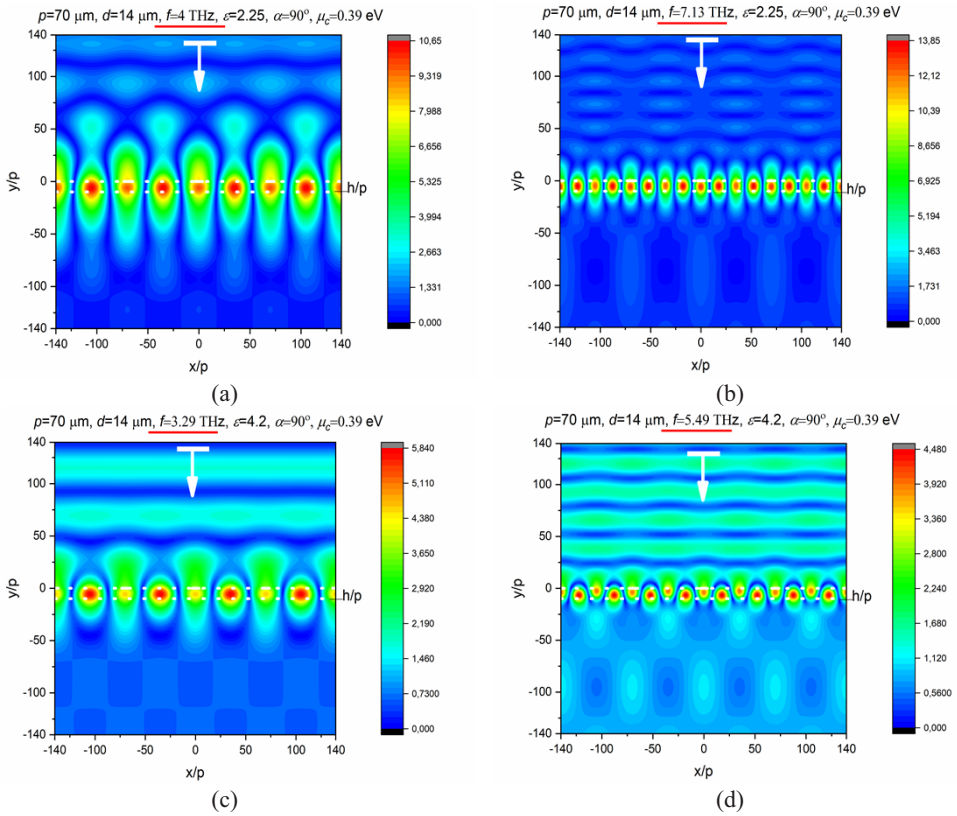

Fig. 3. The electric field patterns on four periods in the resonances on the lattice modes L_{10}^{+} ((a) and (c)) and L_{20}^{+} ((b) and (d)) at the normal incidence for the same grating as in Fig. 2. The metasurface parameters are indicated at the top of each panel.

For completeness, in Fig. 4 we show the near electric field patterns at the resonance frequencies, corresponding to the slab mode, S_1. They demonstrate the standing wave patterns in the normal direction only, slightly perturbed by the presence of strips. This is as expected as the bare slab modes are essentially the modes of 1-D Fabry-Perot etalon.

The most famous and attractive for application feature of graphene is the tunability of its electron conductivity and hence its impedance, with the aid of DC bias, which controls the chemical potential – see (14). Therefore, it is interesting and important to study how the variation of the chemical potential translates to the change of the reflectance, transmittance and absorbance of the patterned graphene configuration. As known, in the case of the H-polarization (magnetic field is parallel to the strip edges) the grating of graphene strips possesses the strip plasmon modes [7–14]. Plasmon mode frequencies strongly depend on the chemical potential because these modes are the natural modes of the Fabry-Perot resonator, where graphene surface wave bounces between the strip edges. The propagation constant of the graphene plasmon wave is determined by graphene's impedance, hence, it scales as the square root of the chemical impedance. Thanks to this effect, on-substrate graphene strip gratings are in the core of the design of tunable bio and chemo-sensors [3] based on the measurement of the plasmon-mode resonance peak frequency. The other H-polarization natural modes of such a grating are the slab modes and the lattice modes, which are much less sensitive to the chemical potential variation.

However, in the E-polarization regime, there is no plasmon natural wave on a sheet of graphene and, therefore, no plasmon modes on the strips. This leaves only the slab and the lattice modes as

Optical Materials EXPRESS

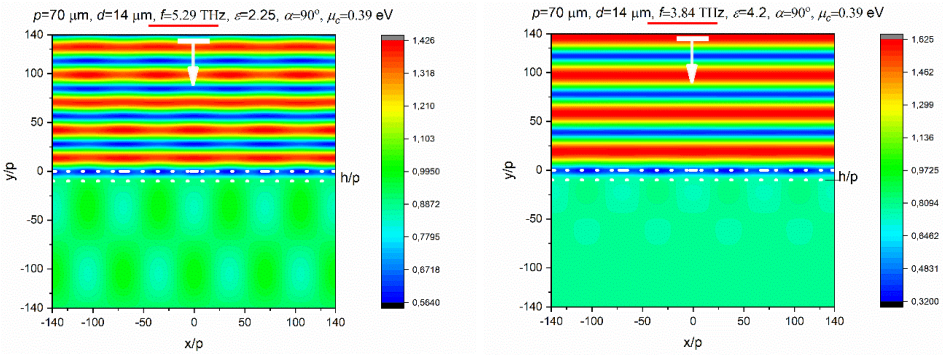

(a) (b)

Fig. 4. The electric field patterns on four periods in the resonances on the slab mode of substrate, S_1, perturbed by the strips, at the normal incidence on the same grating as in Fig. 2 with (a) $\varepsilon = 2.25$ at $f = 5.29$ THz and (b) $\varepsilon = 4.2$ at $f = 3.84$ THz.

possible candidates for the sensor applications. In Fig. 5, we present the plots of R and A versus the frequency at four values of the chemical potential between 0.25 eV and 1 eV.

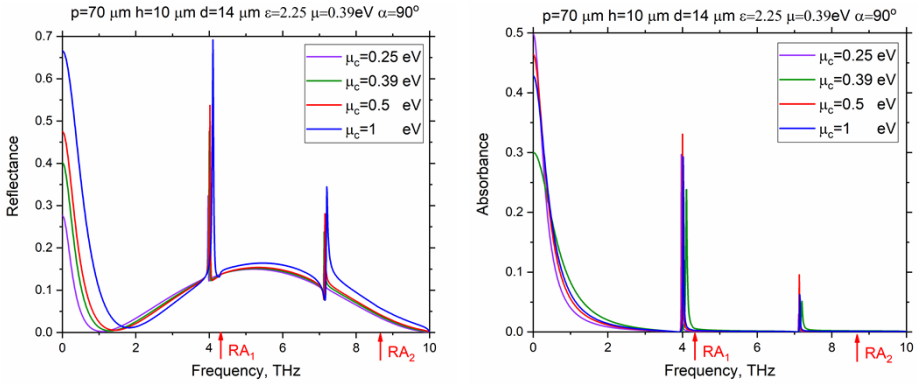

(a) (b)

Fig. 5. Reflectance (a) and absorbance (b) versus the frequency at the normal incidence on the same grating as in Figs. 2 at four values of chemical potential, $\mu_c = 0.25$ eV, 0.39 eV, 0.5 eV and 1 eV.

These plots show that the variation of the chemical potential still has certain effect on the lattice-mode resonances. To obtain clearer vision of this tunability, we present in Fig. 6 the color maps of the reflectance and absorbance as functions of two parameters, frequency and chemical potential. On these maps, the lattice-mode resonances show up as bright narrow "ridges" of high reflection located on the red side from the RA frequencies (marked with arrows) and approaching these frequencies as the chemical potential grows up.

Note that this is in contrast to the *enhanced transmission* in the lattice-mode resonances that is found in the E-polarization scattering from imperfect-metal strip gratings on dielectric substrate [27]. The difference appears due to good transparency of graphene in the THz range in contrast to nearly impenetrable behavior of thin metal film used in [27] in the sub-THz range. As we explain in the next section, the lattice modes can be studied analytically thanks to the regularized nature of Eq. (12).

Optical Materials EXPRESS

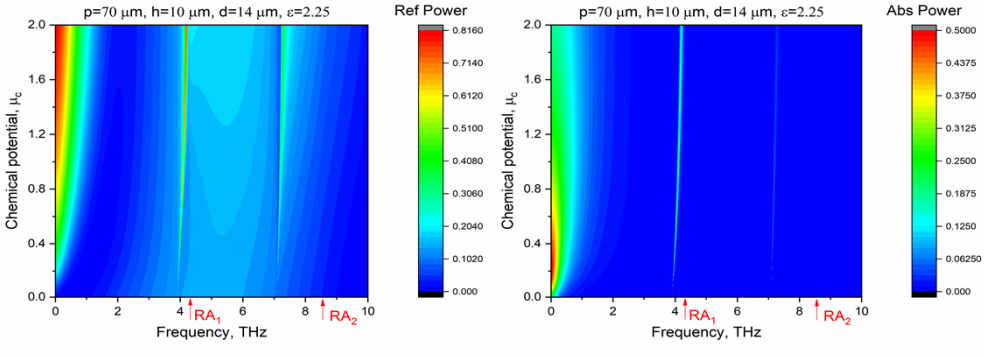

(a) (b)

Fig. 6. Color maps of reflectance (a) and absorbance (b) versus the frequency and the chemical potential at the normal incidence at the same grating as in Figs. 2–5.

5. Analytical characterization of the lattice modes

The casting of the considered full-wave scattering problem to the Fredholm second-kind matrix Eq. (12) enables us to perform analytical study of the lattice modes and associated to them resonances in mathematically grounded manner, i.e. without resorting to the empiric quasi-static and circuit-theory considerations. This follows from the Gershgorin theorem of the matrix algebra [28], which states that the characteristic numbers of such a matrix equation are contained inside finite-radius circles on the complex plane, with their centers at the zeros of the diagonal elements. Here, it is necessary to split the matrix of (12) into two independent matrices, for the x-even and x-odd electromagnetic fields, that leads to replacement of $S_{m,n}$ with the coefficients $S^{\pm}_{m,n}$=$S_{m,n} \pm S_{-m,n}$, respectively. Then, taking into account that at the normal incidence, $\alpha = \pi/2$, only the x-even natural modes can be excited, their approximate characteristic equations are

$$\Delta_m(\kappa) = 1+\frac{\kappa S^{+}_{m,m}}{Z(\kappa)\Gamma_m(\kappa)}+\frac{\kappa^2}{Z^2(\kappa)\Gamma_m(\kappa)}\sum_{n=0,\neq m}^{\infty}\frac{\Gamma_n^{-1}(\kappa)S^{+}_{m,n}S^{+}_{n,m}}{1+\kappa Z^{-1}(\kappa)\Gamma_n^{-1}(\kappa)S^{+}_{n,n}}+O(Z^{-3}) = 0, \quad m = 0, 1, 2, \ldots \tag{19}$$

At first, consider the case of *the graphene strip grating suspended in the free space*, $\varepsilon = 1$. Then, as follows from (9), $\Gamma_m = 2\gamma_m = 2(\kappa^2 - m^2)^{1/2}$, so that the following equation is derived:

$$\gamma_m(\kappa) + \frac{\kappa S^{+}_{m\,m}}{2Z(\kappa)} + O(Z^{-2}) = 0, \quad m = 1, 2, \ldots, \tag{20}$$

where $S^{+}_{m\,m}(s) = s + \sin(2\pi m s)/2\pi m$. However, this equation has no roots in the domain $Re\kappa<m$. Indeed, if we assume for simplicity that graphene is lossless, $1/\tau = 0$, and that $f<f_c$ (i.e. the intraband conductivity dominates over the interband one), then we can characterize its impedance with expression (17). After some algebra, we obtain equation

$$i\sqrt{m^2 - \kappa^2} + i\frac{p\Omega}{4\pi c}S^{+}_{mm}(s) + O(Z^{-2}) = 0, \quad m = 1, 2, \ldots, \tag{21}$$

that has no roots with $Re\kappa<m$ on the top sheet of the square-root function involved (although such a root is present on the bottom sheet, it does not show up in the reflectance spectra).

Returning to *the graphene strip grating located on the surface of dielectric substrate*, one has to use full expression (9) for Γ_m, so that, if $f<f_c$, then

$$\Gamma_m(\kappa) + i\frac{p\Omega S^{+}_{m\,m}(s)}{\pi c}\left(1 + \frac{ip}{2\pi c\tau}\right) + O(Z^{-2}) = 0, \quad m = 1, 2, \ldots \tag{22}$$

Optical Materials EXPRESS

In Fig. 7, we present zooms of the color maps of the reflectance from Fig. 6-(a) near the lattice-mode resonances $L_{10}{}^{+}$ and $L_{20}{}^{+}$.

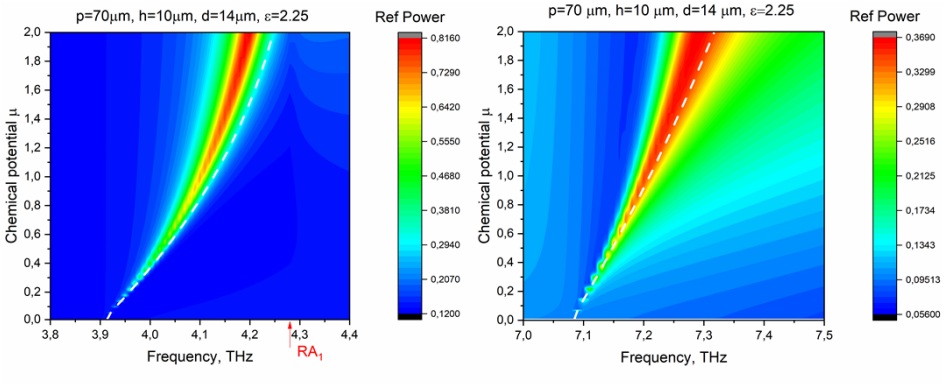

(a) (b)

Fig. 7. Zooms of color map of reflectance from Fig. 6-(a) near the lattice-mode resonances $L_{10}{}^{+}$ and $L_{20}{}^{+}$. Dashed white lines show the frequencies found from approximate Eq. (22).

Here, we have added, by white dashed lines, the solutions of approximate equations (22), where it is assumed that $1/\tau = 0$, truncated to $N = 50$. One can see very close agreement between the peak values of R and the real parts of the corresponding lattice-mode frequencies.

The expression for $\Gamma_m(\kappa)$ is quite complicated, however, it can be simplified under the assumption that the substrate is electrically thin, i.e. $h/\lambda \to 0$, namely,

$$\Gamma_m = 2\gamma_m - i\xi(\varepsilon - 1)\kappa^2 + O(\xi^2) \tag{23}$$

Then, assuming again that $f < f_c$, we obtain the following approximate characteristic equation instead of (21):

$$\gamma_m(\kappa) - \frac{i}{2}\xi(\varepsilon - 1)\kappa^2 + i\frac{p\Omega S^{+}_{m\,m}(s)}{2\pi c}\left(1 + \frac{ip}{2\pi c\tau}\right) + O(\xi^2, Z^{-2}) = 0, \quad m = 1, 2, \ldots, \tag{24}$$

This equation can be treated analytically in the same way as (20). The result is

$$\kappa^{L+}_{m0} = m - \frac{m}{8}\xi(\varepsilon - 1)\left[m^2\xi(\varepsilon - 1) - \frac{2p\Omega S^{+}_{m\,m}(s)}{\pi c}\right] + i\frac{\xi(\varepsilon - 1)p^2\Omega S^{+}_{m\,m}(s)}{4\pi^2 m^2 c^2 \tau} + O(\xi^3, \tau^{-2}, Z^{-2}) = 0, \tag{25}$$

Therefore, unlike the case of suspended grating, if the parameters of the dielectric substrate, ε and h, are fixed, however the strips are vanishing, $s \to 0$, then the lattice-mode complex natural frequencies tend to the real numbers, which are redshifted from the RA frequencies,

$$\kappa^{L+}_{m0} \to m - \tfrac{1}{8}m^3(\varepsilon - 1)^2\xi^2 \tag{26}$$

As one can verify, Eq. (25) corresponds to the condition that the grating period equals to m wavelengths of the principal guided wave of the dielectric slab TE_0, which has no cutoff frequency. Indeed, this wave propagation constant, g_{TE0}, satisfies the transcendental equation, $\tan\left(\frac{1}{2}\sqrt{k^2\varepsilon - g^2_{TE0}}h\right) = \sqrt{g^2_{TE0} - k^2}/\sqrt{k^2\varepsilon - g^2_{TE0}}$. This equation can be solved analytically if we replace the tangent function with the leading term of its expansion for $h \to 0$, yielding $\lambda_{TE0} = \lambda\left[1 - \frac{1}{8}k^2h^2(\varepsilon - 1)^2\right] + O(k^3h^3)$ that is in full agreement with (26).

For completeness, it should be noted that if the frequency or the substrate contrast or its thickness gets larger, then, besides the principal wave TE_0, the substrate starts guiding similar

Optical Materials EXPRESS

waves of the higher orders, TE_M, $M > 0$. Therefore, new lattice-mode resonances can be expected, mediated by these higher guided waves as well. This guess is indeed supported by computations (not shown here). Thus, the lattice modes should be classified using not one but two indices, $L^{\pm}_{mM}$, where $m = 1,2,\ldots$ and $M = 0,1,2,\ldots$ while $\pm$ corresponds to the parity in x.

The obtained above expressions show that the frequencies of the lattice-mode resonances of the on-substrate graphene strip grating are always close to the RA frequencies, being red-shifted from them by the value mediated by the guided waves of the substrate. However, lattice-mode resonances are still tunable, although in much narrower band than the frequencies of the plasmon-mode resonances, which exist only in the case of the H-polarized wave scattering. This tunability is visible well on the maps in Fig. 7 where the largest potential is taken as 2 eV.

Another interesting question is the dependence of the lattice-mode resonances of the filling ratio, $s = d/p$. Color maps in Fig. 8 show the reflectance and absorbance as functions of the frequency and s, computed from the full-wave Eq. (12) truncated to $N = 50$.

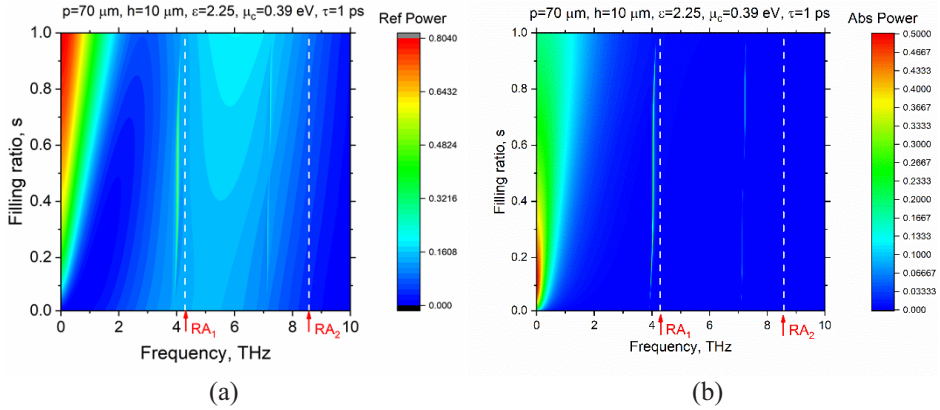

(a) (b)

Fig. 8. Color maps of reflectance (a) and absorbance (b) versus the frequency and the grating filling factor at the normal incidence at the same grating as in Figs. 2–7.

As visible, the lattice-mode resonances remain red-shifted from the RA frequencies for all s, however, this shift gets smaller if $s \to 1$, i.e. if the slots between strips are vanishing. The limiting value of the resonance frequency at $s = 1$ corresponds to the condition that the grating period equals m lengths of the natural wave, guided by the substrate with the upper surface covered with graphene.

In Fig. 9, we present the zooms of the color map of the reflectance from Fig. 8-(a) in the vicinities of three lattice-mode resonances, $L_{10}{}^{+}$, $L_{20}{}^{+}$ and $L_{30}{}^{+}$. computed from the full-wave Eq. (12) truncated to $N = 50$. For comparison, dashed white lines show the resonance frequencies found from approximate Eq. (22), where it is assumed that $1/\tau = 0$.

One can see very good agreement between these approximations and the peak values of R. Note that the number of the peak broadenings corresponds to the mode index. These broadenings are caused by the drops in the mode Q-factors, which correlate with the overlap of the lossy strip with the lattice-mode E-field, see Fig. 4.

Finally, we see that the Q-factors of the lattice modes, defined as $Q^{L+}_{m0} = -Re\kappa^{L+}_{m0}/2\mathrm{Im}\kappa^{L+}_{m0}$, are given by

$$Q^{L+}_{m0} = \frac{2\pi^2 m^3 c^2 \tau}{\xi(\varepsilon-1)p^2\Omega S^{+}_{m\,m}(s)}\left\{1 - \frac{1}{8}\xi(\varepsilon-1)\left[m^2\xi(\varepsilon-1) - \frac{2p\Omega S^{+}_{m\,m}(s)}{\pi c}\right]\right\}, \quad m = 1,2,\ldots \tag{27}$$

Now, if we assume that the strips are narrow, so that the filling ratio is small, $s = \theta/\pi = d/p \to 0$, then for all m and n $S^{+}_{m,n}(s) = 2s + O(s^3)$, and hence then the complex natural frequencies of the

Optical Materials EXPRESS

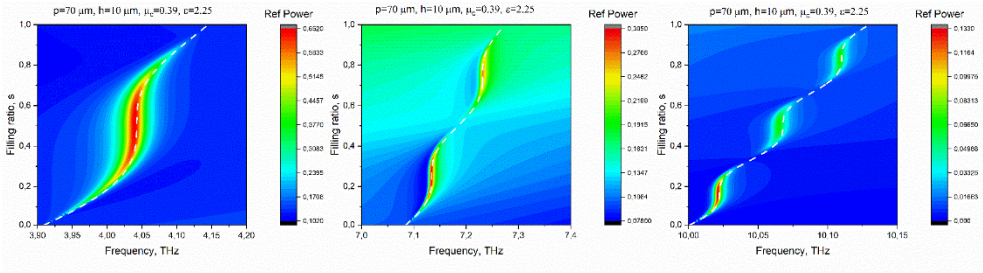

Fig. 9. Zooms of color map of reflectance from Fig. 8-(a) near the lattice-mode resonances $L_{10}{}^{+}$ (a), $L_{20}{}^{+}$ (b) and $L_{30}{}^{+}$ (c); the frequencies of RAs, which correspond to $\kappa = 1$, 2 and 3 at the normal incidence are 4.286 THz, 8.572 and 12.857 THz. Dashed white lines show the resonance frequencies found from approximate Eq. (22).

lattice modes tend to real numbers that entails unlimited growth of Q_{m0}^{L+}. The same happens if the substrate vanishes, i.e. if either $\varepsilon \to 1$ or $h \to 0$. At arbitrary s, dependences of Q-factors on s correlate with the overlap between the lossy graphene strip and the mode electric field magnitude.

For instance, if $p = 70\ \mu$m, $h = 1\ \mu$m, $d = 14\ \mu$m, $T = 300$ K, $\tau = 1$ ps and $\mu_c = 0.25$ eV, then $f_{10}^{L+} = 4.3124$ and $Q_{10}^{L+} = 431.15$ while if it is 1 eV, then $f_{10}^{L+} = 4.2857$ and $Q_{10}^{L+} = 107.79$.

6. Conclusions

We have used the mathematically grounded MAR-IDFT technique to study numerically the scattering and absorption of terahertz-range electromagnetic plane wave by the metasurface shaped as array of graphene strips on flat dielectric substrate. Unlike commercial codes, this technique guarantees the convergence of numerical results to the true solution if the discretization order gets larger. Thanks to the absence of numerical integrations needed to fill in the matrix, our in-house code is not only accurate but also very fast. With the aid of this trusted and efficient modelling instrument, we have analyzed the effect of the resonances, in the range of frequencies from zero to 10 THz, caused by the E-polarized natural modes of two types: slab modes of the substrate and lattice modes of the whole configuration as a periodic open resonator.

Additionally, assuming that the substrate is lossless but graphene strips are lossy, we have derived the mathematically grounded full-wave asymptotic expressions for the lattice mode complex frequencies and Q-factors. These expressions are in good agreement with numerical results.

This analysis shows that the E-polarized lattice modes do not exist if the graphene strip grating is suspended in the free space. If the grating is supported by a whatever thin dielectric substrate, their complex-frequency poles are close, from the red side, to the Rayleigh Anomalies, which are the field function branch points. The shift from RAs is controlled by the wave length of the principal guided wave of the dielectric slab substrate. This means that the lattice-mode Q-factors grow up infinitely if strips get narrower or if the substrate gets thinner or if substrate's contrast with the host medium vanishes.

Remarkably, the lattice-mode frequencies are still tunable with the aid of the graphene chemical potential, although within much narrower range than that of the strip plasmon modes of the same grating in the case of the H-polarization.

Note that, even if the substrate is moderately thin, say, has the thickness of 1 μm, the lattice-mode Q-factors can reach 10^5, so that the numerical solutions must deliver 5 or more correct digits. Such high accuracy is not accessible with any existing today commercial code, however can be provided by our developed above MAR-IDFT code.

Optical Materials EXPRESS

Funding. National Research Foundation of Ukraine (#2020-02-150).

Disclosures. The authors declare no conflicts of interest.

Data availability. All computations relating to Eq. (12) may be readily reproduced by the reader by using the expressions and formulas explicitly provided in the paper.

References

1. F. Javier García de Abajo, "Graphene plasmonics: challenges and opportunities," ACS Photonics **1**(3), 135–152 (2014).
2. T. Low and P. Avouris, "Graphene plasmonics for terahertz to mid-infrared applications," ACS Nano **8**(2), 1086–1101 (2014).
3. D. Rodrigo, O. Limaj, D. Janner, D. Etezadi, F. J. Garcia de Abajo, V. Pruneri, and H. Altug, "Mid-infrared plasmonic biosensing with graphene," Science **349**(6244), 165–168 (2015).
4. Z. Ullah, G. Witjaksono, I. Nawi, N. Tansu, M. I. Khattak, and M. Junaid, "A review on the development of tunable graphene nanoantennas for terahertz optoelectronic and plasmonic applications," Sensors **20**(5), 1401 (2020).
5. G. W. Hanson, "Dyadic Green's functions and guided surface waves for a surface conductivity model of graphene," J. Appl. Phys. **103**(6), 064302 (2008).
6. W. Fuscaldo, P. Burghignoli, P. Baccarelli, and A. Galli, "Efficient 2-D leaky-wave antenna configurations based on graphene metasurfaces," Int. J. Microw. Wireless Techn. **9**(6), 1293–1303 (2017).
7. R.-B. Hwang, "A theoretical design of evanescent wave biosensors based on gate-controlled graphene surface plasmon resonance," Sci. Rep. **11**(1), 1999 (2021).
8. O. V. Shapoval, J. S. Gomez-Diaz, J. Perruisseau-Carrier, J. R. Mosig, and A. I. Nosich, "Integral equation analysis of plane wave scattering by coplanar graphene-strip gratings in the THz range," IEEE Trans. Terahertz Sci. Technol. **3**(5), 666–674 (2013).
9. T. L. Zinenko, A. Matsushima, and A. I. Nosich, "Surface-plasmon, grating-mode and slab-mode resonances in THz wave scattering by a graphene strip grating embedded into a dielectric slab," IEEE J. Sel. Top. Quantum Electron. **23**(4), 1–9 (2017).
10. T. L. Zinenko, A. Matsushima, and A. I. Nosich, "Terahertz range resonances of metasurface based on double grating of microsize graphene strips inside dielectric slab," Proc. R. Soc. A. **476**(2240), 20200173 (2020).
11. M. E. Kaliberda, L. M. Lytvynenko, and S. A. Pogarsky, "THz waves scattering by finite graphene strip grating embedded into dielectric slab," IEEE J. Quantum Electronics **56**(1), 1–7 (2020).
12. M. E. Kaliberda, L. M. Lytvynenko, and S. A. Pogarsky, "Singular integral equations analysis of THz wave scattering by an infinite graphene strip grating embedded into a grounded dielectric slab," J. Opt. Soc. Am. A **36**(10), 1787–1794 (2019).
13. F. O. Yevtushenko, S. V. Dukhopelnykov, T. L. Zinenko, and Y. G. Rapoport, "Electromagnetic characterization of tuneable graphene strips-on-substrate metasurface over entire THz range: Analytical regularization and natural-mode resonance interplay," IET Microwaves Antennas Propagat. **15**(10), 1225–1239 (2021).
14. A. Khavasi, "Ultra-sharp transmission resonances in periodic arrays of graphene ribbons in TE polarization," J. Lightwave Technol. **34**(3), 1020–1024 (2016).
15. A. I. Nosich, "Method of analytical regularization in computational photonics," Radio Sci. **51**(8), 1421–1430 (2016).
16. T. L. Zinenko, A. I. Nosich, and Y. Okuno, "Plane wave scattering and absorption by resistive-strip and dielectric-strip periodic gratings," IEEE Trans. Antennas Propag. **46**(10), 1498–1505 (1998).
17. A. Matsushima, T. Fujimura, and T. Itakura, "Scattering of an arbitrary plane wave by an infinite strip grating loaded with a pair of dielectric slabs," J. Electromagnetic Waves and Applications **7**(6), 791–809 (1993).
18. F. Mesa, L. Jelinek, F. Medina, and R. Marqués, "Analytical theory of extraordinary transmission through metallic diffraction screens perforated by small holes," Opt. Express **17**(7), 5571–5579 (2009).
19. F. Medina, F. Mesa, and D. C. Skigin, "Extraordinary transmission through array of slits: circuit theory model," IEEE Trans. Microwave Theory Techn. **58**(1), 105–115 (2010).
20. A. Hessel and A. A. Oliner, "A new theory of Wood's anomalies on optical gratings," Appl. Opt. **4**(10), 1275–1297 (1965).
21. V. Lomakin and E. Michielssen, "Transmission of transient plane waves through perfect electrically conducting plates perforated by periodic arrays of subwavelength holes," IEEE Trans. Antennas Propag. **54**(3), 970–984 (2006).
22. V. O. Byelobrov, T. L. Zinenko, K. Kobayashi, and A. I. Nosich, "Periodicity matters: grating or lattice resonances in the scattering by sparse arrays of sub-wavelength strips and wires," IEEE Antennas Propag. Mag. **57**(6), 34–45 (2015).
23. V. V. Yachin, T. L. Zinenko, and S. V. Mizrakhy, "Resonance enhancement of Faraday rotation in double-periodic gyromagnetic layers analyzed by the method of integral functional," J. Opt. Soc. Am. B **35**(4), 851–860 (2018).
24. V. G. Kravets, A. V. Kabashin, W. L. Barnes, and A. N. Grigorenko, "Plasmonic surface lattice resonances: a review of properties and applications," Chem. Rev. **118**(12), 5912–5951 (2018).
25. A. D. Utyushev, V. I. Zakomirnyi, and I. L. Rasskazov, "Collective lattice resonances: plasmonics and beyond," Rev. Phys. **6**, 100051 (2021).

Optical Materials EXPRESS

26. D. O. Herasymova, S. V. Dukhopelnykov, D. M. Natarov, T. L. Zinenko, M. Lucido, and A. I. Nosich, "Threshold conditions for transversal modes of tunable plasmonic nanolasers shaped as single and twin graphene-covered circular quantum wires," Nanotechnology **33**(49), 495001 (2022).
27. S. Freer, M. Camacho, S. A. Kuznetsov, R. R. Boix, M. Beruete, and M. Navarro-Cia, "Revealing the underlying mechanisms behind TE extraordinary THz transmission," Photonics Res. **8**(4), 430–439 (2020).
28. R. S. Varga, *Geršgorin and His Circles* (Springer Series in Computational Mathematics), vol. 36. (Springer, 2004.